

Charge transport in TiO₂/MEH-PPV polymer photovoltaics

A. J. Breeze, Z. Schlesinger, and S. A. Carter*

Physics Department, University of California, Santa Cruz, California 95064

P. J. Brock

IBM Almaden Research Center, San Jose, California

(Received 5 June 2000; revised manuscript received 28 November 2000; published 10 September 2001)

We study the effect of polymer thickness, hole mobility, and morphology on the device properties of polymer-based photovoltaics consisting of MEH-PPV as the optically active layer, TiO₂ as the exciton dissociation surface, and ITO and Au electrodes. We demonstrate that the conversion efficiency in these polymer-based photovoltaics is primarily limited by the short exciton diffusion length combined with a low carrier mobility. For MEH-PPV devices with optimal device geometry, we achieve quantum efficiencies of 6% at the maximum absorption of the polymer, open circuit voltages of 1.1 V, current densities of 0.4 mA/cm² and rectification ratios greater than 10⁵ under 100 mW/cm² white light illumination. In addition, we achieve fill factors up to 42% at high light intensities and as high as 69% at low light intensities. We conclude by presenting a model that describes charge transport in solid-state polymer/TiO₂-based photovoltaics and suggest methods for improving energy conversion efficiencies in polymer-based photovoltaics.

DOI: 10.1103/PhysRevB.64.125205

PACS number(s): 85.60.Dw, 73.61.Ph

I. INTRODUCTION

Over the last decade, polymer-based semiconductors have emerged as a novel class of optoelectronic materials that combine the potential of high power efficiency with inexpensive liquid based processing over large areas. Significant effort in this field has focused on improving the material purity and optoelectronic properties as well as understanding the injection and transport properties of electrons, holes, and excitons in semiconducting polymers. As a partial consequence of this effort, polymer light emitting diodes (LED's) have recently achieved quantum and power efficiencies comparable to inorganic LED's and are now on the brink of commercialization. Nonetheless, while charge injection and exciton recombination has been well studied in polymer-based semiconductors, the reverse process, namely charge generation and exciton dissociation, has yet to be as well understood and optimized. Recently, several groups have achieved power efficiencies for polymer-based solar cells approaching 4% conversion efficiency over the absorption region of the polymer using either polymer-polymer or polymer-nanoparticle blends to improve exciton dissociation.¹⁻³ While this work is encouraging, the quantum efficiencies are still significantly below either amorphous silicon or dye-sensitized electrochemical cells.⁴ Moreover, a significant amount of photon-aided charge injection, trapping, and recombination can occur in polymer-based photovoltaics, making the interpretation of the electrical data (i.e., the current-voltage characteristics) difficult.⁵

In this paper, we focus on understanding the mechanisms for charge generation, transport, and exciton dissociation in poly (2-methoxy,5-(2'-ethyl-hexyloxy)-*p*-phenylenevinylene) (MEH-PPV) polymer-based photovoltaic devices in a dry nitrogen atmosphere where charge injection in the forward bias has been substantially reduced using a TiO₂ barrier. Although MEH-PPV is not the most efficient photovoltaic material, we have chosen it for these studies because it is

well characterized and highly reproducible with a low intrinsic trap density.⁶ We study the electrical characteristics and photoaction current spectra for TiO₂/MEH-PPV devices with indium tin oxide (ITO) and Au contacts as a function of polymer thickness, polymer mobility, and the morphology of the TiO₂/polymer interface. We find for optimal device geometry a quantum efficiency of 6% at the maximum absorption of the polymer, open circuit voltages of 1.1 V, current densities of 0.4 mA/cm², fill factors of 42% and rectification ratios greater than 10⁵ under 100 mW/cm² white light illumination. Our results on nonblended MEH-PPV based devices are comparable to results for electron-transporting polymers and nanoparticles blended into MEH-PPV.^{1,2} We propose a charge transport model to understand our results and discuss the ramifications of this model for achieving higher power efficiencies in polymer-based photovoltaics.

II. EXPERIMENT

Photovoltaic devices of the structure ITO/TiO₂ sol-gel/MEH-PPV/Au, as shown in Fig. 1, are constructed by spinning down first a titanium dioxide (TiO₂) sol-gel and then the photoactive polymer MEH-PPV over indium tin oxide (ITO) patterned glass. The TiO₂ sol-gel is formed via a precursor solution, as described elsewhere.⁷ After being spun cast, the sol-gel is heated under vacuum (~25 in Hg) at 125 °C for 1 h to bake out solvents and other impurities. For sintered layers, the slide is then baked at 450 °C under atmospheric pressure for another hour in order to convert the film structure to crystalline anatase. As an alternative to the sol-gel film, a solution of 13-nm diameter anatase TiO₂ nanoparticles suspended in water is deposited via spin casting and annealed at 450 °C for 1 h. The slide is next brought into a dry nitrogen atmosphere glove box and cleaned prior to the deposition of the MEH-PPV polymer (in *p*-xylene solvent) via spin coating. The thickness of the polymer layer is controlled both by spin speed and by the concentration of poly-

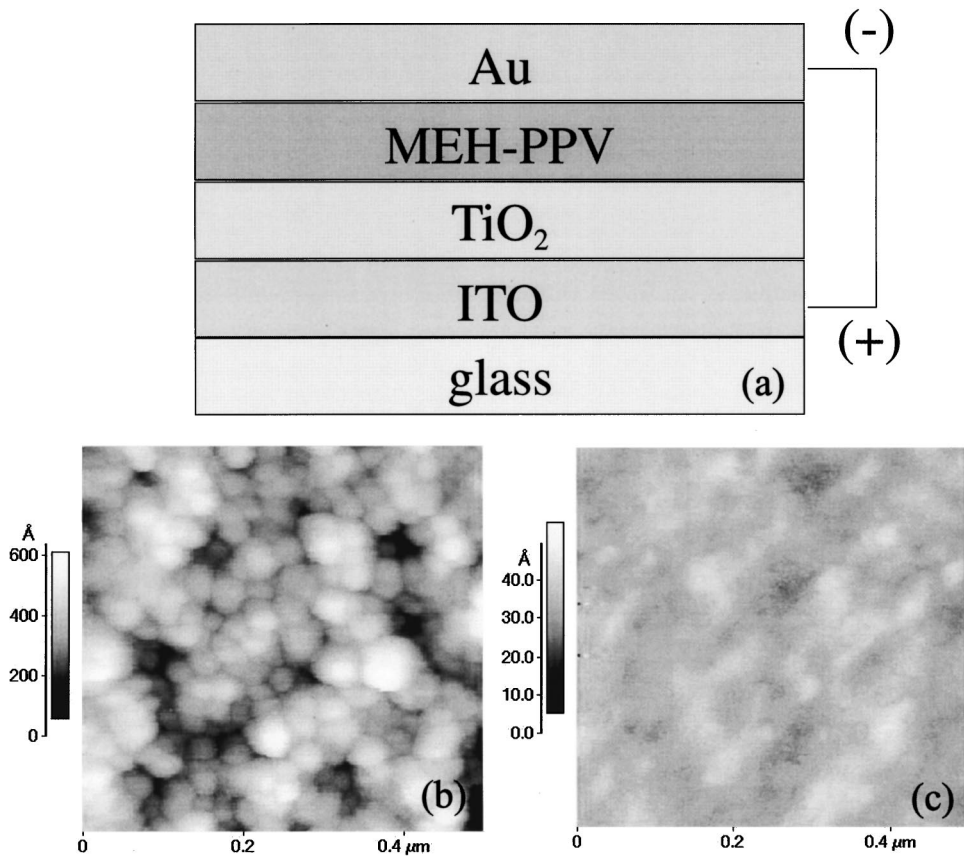


FIG. 1. (a) A side view of the layered structure for the ITO/TiO₂/MEH-PPV/Au devices. (b) An AFM image of a TiO₂ nanoparticle layer. (c) An AFM image of a sintered TiO₂ sol-gel layer.

mer in the solvent with average values of 2000 rpm and 0.8% by weight, respectively. We test two different procedures for removing the solvent from the polymer film. The first method, annealing, requires heating the slide overnight at 100 °C and then placing it in a vacuum on the order of 10^{-6} torr for 2 h before evaporating the gold patterned electrode over the polymer film. For the nonannealing technique, the slide is placed in the same vacuum overnight before the deposition of the gold contact. For comparison purposes, devices of the type ITO/PEDT/MEH-PPV/Al are constructed in a similar fashion, with the poly (ethyldioxy-thiophene) PEDT film deposited by the spin casting method.⁸ All device areas are 3 mm² with six devices per substrate to check reproducibility.

The thicknesses of both the TiO₂ and the polymer films are determined using an atomic force microscope (AFM) in contact mode. Thicknesses for the MEH-PPV range from 63 to 200 nm. The TiO₂ sol-gel and nanoparticle films are 50 and 300 nm thick, respectively. We also use AFM to measure the roughness of the TiO₂ films. Both sintered and nonsintered sol-gel films are very smooth, with variations on the order of only 2 nm [Fig. 1(c)]. Contrasted to this are the rough nanoparticle layers that have variations up to 100 nm [Fig. 1(b)]. The thickness of the gold electrode, measured during evaporation via a crystal monitor, is 25 nm.

Electronic transport in the ITO/TiO₂/MEH-PPV/Au devices is studied via current density voltage (J - V) curves, taken using a 2400 Keithley source meter by sourcing voltage across the ITO (positive) and gold (negative) electrodes and measuring the resulting current density. Due to the re-

versed internal field, measurements on the ITO/PEDT/MEH-PPV/Al devices are taken by sourcing ITO negative and Al positive. The voltage is sourced from -1.0 to 1.0 V in 0.02 V steps. These J - V curves are taken both in the dark and under white illumination provided by a halogen source through the ITO electrode. Light intensities vary from 5 to 220 mW/cm².⁹

Photoaction current spectra are taken at zero bias using a halogen light source, monochromator, chopper, and lock-in amplifier, as described elsewhere.¹⁰ To prevent oxygen from diffusing into the polymer layer and creating additional charge traps, the devices are transferred out of the glovebox inside of a sealed test chamber. They therefore remain under the same dry nitrogen atmosphere throughout the photoaction current spectra measurements. Reference spectra are taken using a calibrated silicon solar cell. Absorption spectra are taken with an N & K optical spectrometer.

III. RESULTS

For devices of the type ITO/TiO₂/photoactive polymer/Au, the open circuit voltage V_{oc} (i.e., the applied voltage at which the current density is zero) under illumination is determined by the difference between the quasi-Fermi energy level of the TiO₂ (~ 4.2 eV) and the work function of the Au electrode or the HOMO level of the MEH-PPV.^{4,7} In our system, the Au electrode (work function 5.1 eV) forms a nearly Ohmic contact with the HOMO of MEH-PPV (5.3 eV). Such devices exhibit low dark current densities in forward bias as well as a saturation of the photocurrent density

in forward bias under illumination. The exciton dissociation occurs at the TiO₂-polymer interface, with transfer of the electron to the TiO₂ as the important process for charge collection.^{7,10} Moreover, TiO₂ serves as an effective hole blocker.

Our focus in this paper is to understand what determines the energy conversion (or power) efficiencies in polymer-based photovoltaic devices consisting of a TiO₂ layer as the main exciton dissociation site with MEH-PPV as the photoactive polymer semiconductor. Our results consist of measurements where we have modified the polymer thickness, the polymer morphology through annealing, and the surface roughness of the TiO₂ layer. Such changes are expected to systematically probe the effects of internal resistance, polymer hole mobility, and surface area of the exciton dissociation site on the charge transport properties of polymer-based photovoltaics.

A. Polymer thickness

Open circuit voltage (V_{oc}), short circuit current density (J_{sc}), and the fill factor are measured for polymer thicknesses of 63, 75, 95, and 200 nm for the ITO/sintered TiO₂ sol-gel/MEH-PPV/Au devices by examining the J - V curves. The short circuit current density is measured at zero applied bias, while the fill factor is the maximum power delivered to an external load, normalized by the values of J_{sc} and V_{oc} :

$$\text{fill factor (ff)} = (V \times J)_{\text{max}} / (V_{oc} \times J_{sc}).$$

Under white light conditions, the energy conversion efficiency η_p is given by

$$\eta_p = J_{sc} * \text{ff} * V_{oc} / I_v,$$

where I_v is the intensity of incident light. The short circuit current density depends directly on the external quantum efficiency, the number of carriers collected/number of incident photons.

On average, the thinner polymer devices (63 and 75 nm) have short circuit currents up to 150 $\mu\text{A}/\text{cm}^2$ at white-light intensities near 100 mW/cm^2 , while averages for the thicker devices (200 nm) are approximately half that value. Qualitatively, it is possible to understand why the current density increases with decreasing polymer thickness, conversely to the fraction of absorbed light. Although an increase in the thickness of the photoactive layer leads to greater absorption and exciton generation, it is generally only the excitons generated within the diffusion length, 20 ± 3 nm,¹¹ of either of the electrode-polymer interfaces that are able to contribute to the current density. Other excitons produced deeper within the polymer recombine or are trapped before they can exit the device. Once the exciton has been dissociated, one charge is immediately transferred to the close electrode while the remaining one must transverse the polymer layer to reach the opposite electrode. Because of this, thinner layers, with correspondingly fewer traps and fewer chances for recombination, allow more current to exit the device. Our results are in agreement with previous work¹² although we observe a less dramatic effect because the exciton dissociation in our

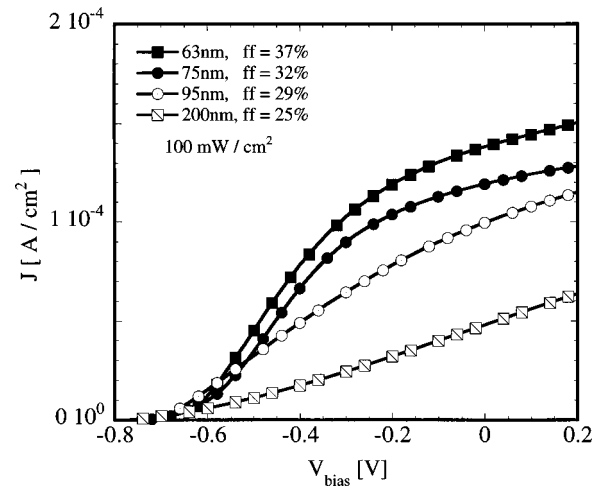


FIG. 2. Current density as a function of applied voltage for devices of the type ITO/sintered TiO₂ sol-gel/MEH-PPV/Au. Polymer MEH-PPV thicknesses are 63 nm (closed squares), 75 nm (closed circles), 95 nm (open circles), and 200 nm (open squares).

devices is occurring at the transparent electrode and because our thicknesses are well above the exciton diffusion length.

In addition, one must take into account the attenuation of light within the polymer. Due to an attenuation length on the order of 110 nm, only a fraction of the incident light reaches the polymer-gold interface. Approximately half the light is transmitted for the thinner devices and about 16% for the thicker 200 nm devices. For this reason, as well as mobility reasons discussed below, it is mainly the dissociation at the TiO₂-polymer interface that actively contributes to the current density.

Comparison of the thinner devices with the thicker MEH-PPV device demonstrates that overall the thinner devices have higher fill factors. Fill factors at high light intensity range from 37% for the 63 nm polymer layer device to 25% for the 200 nm device (Fig. 2). The lower fill factor for thicker polymer layers is most likely due to higher resistive losses. A majority of the charge dissociation occurs at the TiO₂-polymer interface and the holes must traverse the thickness of the polymer to reach the opposite electrode. A thicker layer also requires a higher voltage across the device to achieve the same electric field needed to enable exciton dissociation. Figure 3 plots the current density against the applied voltage for these devices on a semilog scale for various light intensities. As one would expect, higher values are seen for both V_{oc} and J_{sc} for higher incident light intensity. Fill factors, however, decrease for higher light intensities.

Improvement in device performance has been observed as devices age. Open circuit voltages and fill factors generally increase as a device ages from a few days to a few months. Since gold does not initially make very good contact to most polymers, these changes are likely due to slow annealing of the gold/polymer interface, creating a better contact and leading to more efficient removal of holes from the device.¹³ Such an effect can be partially simulated by thermal annealing of the gold electrode once it has been evaporated onto the polymer.

Photoaction current spectra are taken at zero bias to mea-

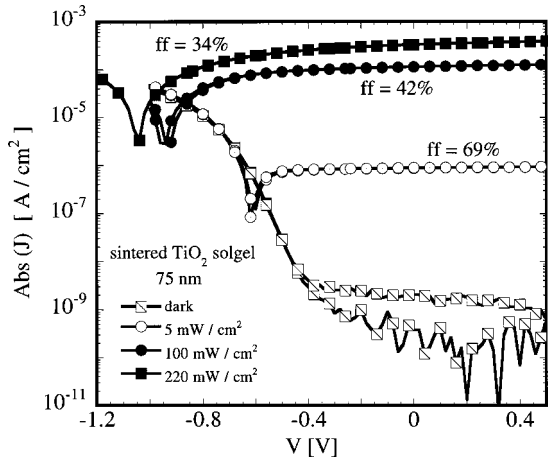


FIG. 3. The absolute value of the current density as a function of applied voltage at various light intensities for an ITO/sintered TiO_2 sol-gel/75 nm MEH-PPV/Au device. Light intensities are approximately 220 mW/cm^2 (closed squares), 100 mW/cm^2 (closed circles), 5 mW/cm^2 (open circles), and dark (open squares).

sure the external quantum efficiency. As can be seen in Fig. 4, quantum efficiencies for the sintered sol-gel devices increase as a function of decreasing polymer thickness, ranging from a 1.6% peak for the 200-nm MEH-PPV layer to a 3.3% peak for the 65-nm layer, consistent with the factor of 2 increase seen for the short circuit current densities. The absorption spectra for MEH-PPV is also shown in Fig. 4 for comparison; the peak device efficiency, located in the range of 498–503 nm, is closely correlated to the peak of 479 nm for the absorption spectrum. This symbioticlike result is expected for a device where the exciton dissociation occurs at the light incident interface. When the exciton dissociating contact is moved to the opposite side of the device as the incident light, such as for ITO/Al electrode devices, the pho-

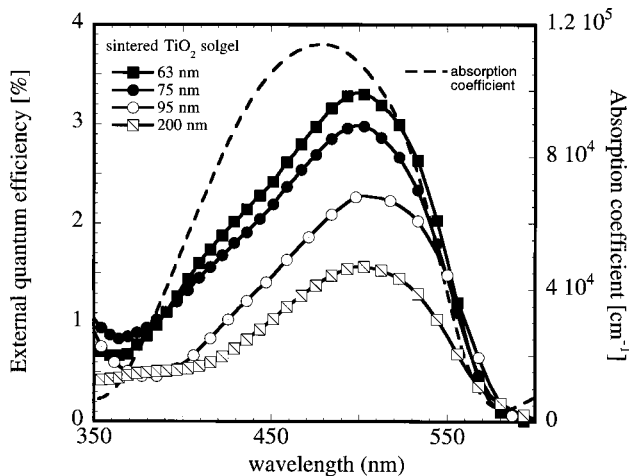


FIG. 4. External quantum efficiency plotted as a function of wavelength for ITO/sintered TiO_2 sol-gel/MEH-PPV/Au devices. Polymer MEH-PPV thicknesses are 63 nm (closed squares), 75 nm (closed circles), 95 nm (open circles), and 200 nm (open squares). The absorption coefficient (dashed line) for MEH-PPV is included for comparison.

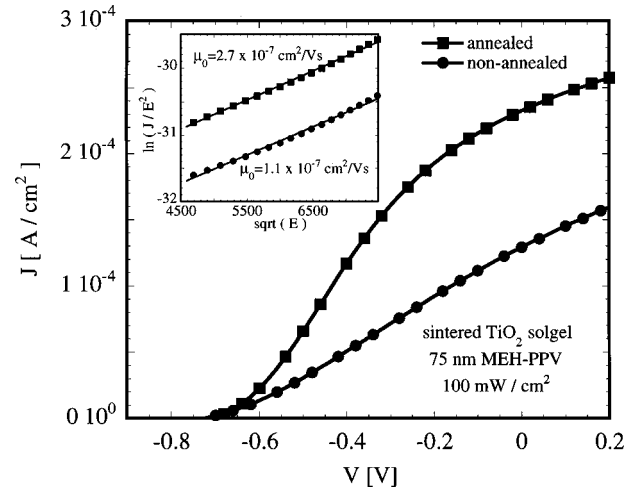


FIG. 5. Current density as a function of applied voltage for annealed and nonannealed MEH-PPV in ITO/sintered TiO_2 sol-gel/MEH-PPV/Au devices. The MEH-PPV layer thickness is 75 nm and the incident light intensity is 100 mW/cm^2 . Inset: Linear fits of $\ln(J/E^2)$ vs $\text{sqrt}(E)$ give the field independent mobility term μ_0 .

toaction current spectra can peak at the absorption edge rather than the absorption maximum.⁷

B. Polymer mobility

Devices with annealed polymer layers have roughly twice the short circuit current density compared to nonannealed devices. Figure 5 shows J - V curves for devices with 75 nm of annealed and nonannealed MEH-PPV. Note that these measurements are for devices only one day old; as explained above, the device performance improves with age. Hole mobility in MEH-PPV is measured for annealed and nonannealed MEH-PPV devices of the type ITO/PEDT/MEH-PPV/Al by taking J - V curves in the range of 5–12 V and fitting the results to a space-charge limited form for a single carrier (Fig. 5 inset),

$$J = 9/8\epsilon\mu E^2/L.$$

Here, E is the electric field across the device, L is the polymer thickness, and a value of $\epsilon = 3.1 \times 10^{-11} \text{ C}^2/(\text{Nm}^2)$ is assumed for the polymer. A Poole-Frenkel-like form, $\mu = \mu_0 \exp[0.89\gamma\text{sqrt}(E)]$, is assumed for the mobility.⁶ Nonannealed devices are found to have an average mobility of $1.1 \times 10^{-7} \text{ cm}^2/\text{Vs}$, while annealed devices average slightly more than twice that at $2.7 \times 10^{-7} \text{ cm}^2/\text{Vs}$. The improvement in polymer mobility with annealing is probably caused by interchain aggregation and partial crystallization in the polymer. Since increasing the mobility can lead to higher exciton dissociation efficiencies, the higher mobility could result in the higher current densities seen in the annealed devices. Annealing does not seem to substantially affect either the open circuit voltage or the fill factor.

C. TiO_2 morphology

Three different forms of TiO_2 were used to investigate the effects of TiO_2 morphology on the device physics and per-

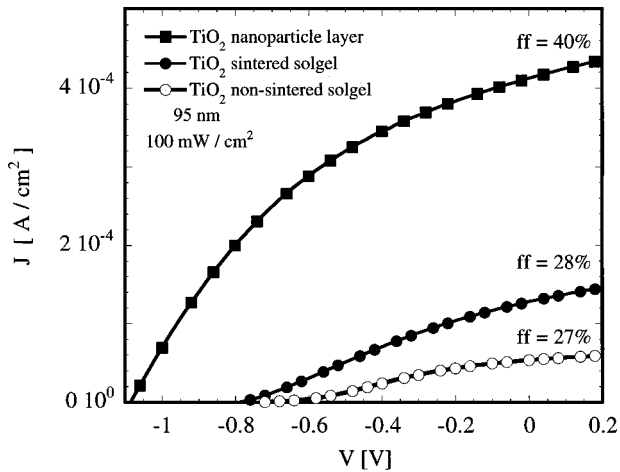


FIG. 6. Current density as a function of applied voltage for ITO/TiO₂/95 nm MEH-PPV/Au devices of various TiO₂ layer morphologies: TiO₂ nanoparticle layer (closed squares), TiO₂ sintered sol-gel (closed circles), and TiO₂ nonsintered sol-gel (open circles). The incident light intensity is 100 mW/cm².

formance: sintered sol-gel, nonsintered sol-gel, and anatase TiO₂ nanoparticle layers.¹⁴ Sintered and nonsintered sol-gel layers are both reasonably smooth, with an average surface roughness of 2 nm compared to the nanoparticle layers that can have as much as a 100 nm peak-to-peak roughness, as shown in Fig. 1.

We observe higher current densities and more than double the external quantum efficiencies for sintered devices compared to their nonsintered counterparts (Figs. 6 and 8). For example, a 95-nm MEH-PPV sintered device has 2.3% peak efficiency while an analogous nonsintered device has only 0.9% peak efficiency (Fig. 8). Since the morphology of the TiO₂ layers are fairly similar, it is likely that these changes are due to a shift in the TiO₂ Fermi energy level during sintering, leading to more efficient exciton dissociation

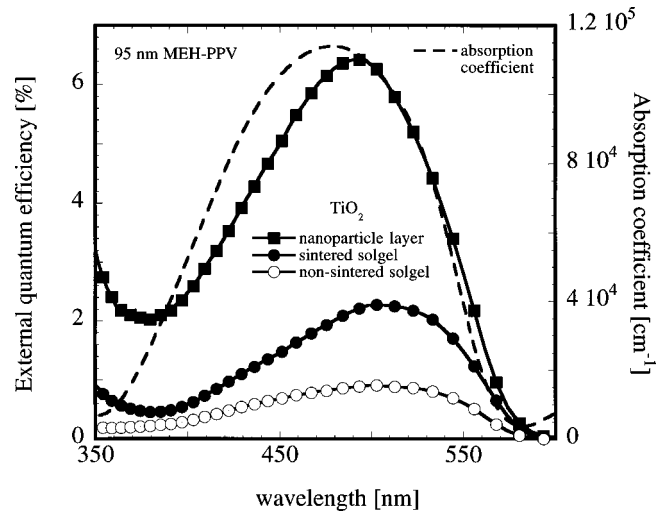


FIG. 8. External quantum efficiency plotted as a function of wavelength for ITO/TiO₂/95 nm MEH-PPV/Au devices of various TiO₂ layer morphologies: TiO₂ nanoparticle layer (closed squares), TiO₂ sintered sol-gel (closed circles), and TiO₂ nonsintered sol-gel (open circles). The absorption coefficient for MEH-PPV is included for comparison.

which is reflected in a slightly higher open circuit voltage. It should be noted, though, that sintering the sol-gel can sometimes subject the layer to small cracks and therefore to partial shorting which increases the dark current and reduces both the open circuit voltage and the fill factor.

Devices made using sintered TiO₂ nanoparticle layers show noticeable improvements in short circuit current density of up to 0.4 mA/cm², open circuit voltages of 1.1 V, and fill factors of 40% at incident light intensity near 100 mW/cm² (Fig. 7). Quantum efficiency is correspondingly improved, with values as high as 6.4% (Fig. 8). These features can likely be explained by considering the rougher surface of the nanoparticle layer as compared to a sol-gel layer. The increased surface area of the dissociation interface leads to higher charge extraction from the device and a subsequent decrease in charge recombination.

D. Comparison with other results

Although TiO₂ layers have been used extensively in dye-sensitized liquid and solid-state solar cells,^{4,15} their use in other types of polymer-based solar cells has been more limited.^{11,16,17} An initial attempt to use a non-dye-sensitized TiO₂ crystalline layer in devices of the type ITO/TiO₂/zinc phthalocyanine (ZnPc)/Au demonstrated that the TiO₂-photoactive material junction showed promise for photovoltaic devices.¹⁵ Later results confirmed that the TiO₂-polymer (PPV and MEH-PPV) interface acts as a dissociation site for excitons generated in the polymer, due to the high electron affinity of the TiO₂ and the low ionization potential of the chosen polymer.^{10,16,17} Arango *et al.* demonstrated that TiO₂ films that suppress electrical contact between the ITO and the polymer take on the role of the electron electrode; rather than the ITO, it is the quasi-Fermi level of the TiO₂ which contributes to the determination of the internal field for the device.¹⁰

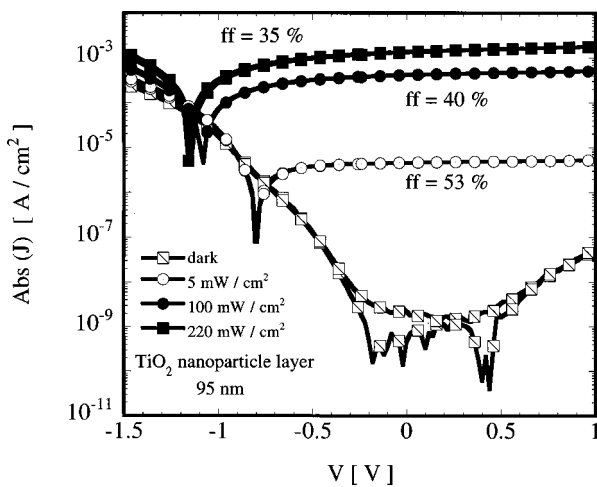


FIG. 7. The absolute value of the current density as a function of applied voltage at various light intensities for ITO/sintered TiO₂ nanoparticles/95 nm MEH-PPV/Au device. Light intensities are 220 mW/cm² (closed squares), 100 mW/cm² (closed circles), 5 mW/cm² (open circles), and dark (open squares).

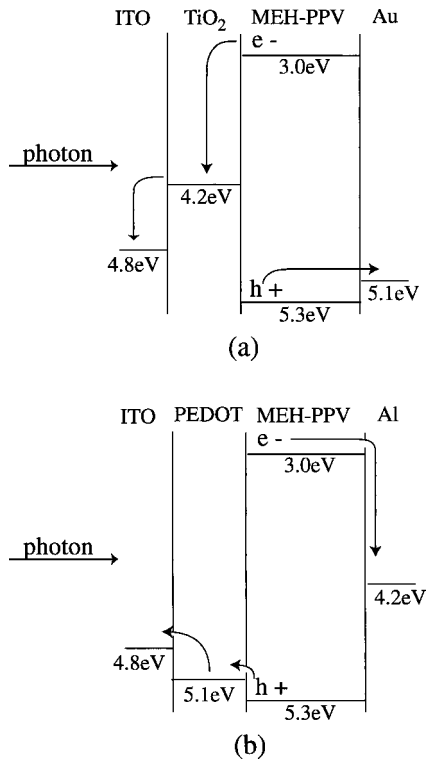


FIG. 9. (a) Flat band energy-level diagram for ITO/TiO₂/MEH-PPV/Au devices. (b) Flat band energy-level diagram for ITO/PEDT/MEH-PPV/Al devices.

Many experiments on homogeneous MEH-PPV polymer photovoltaic devices have used ITO as the semitransparent hole collecting electrode and either aluminum, magnesium, or calcium as the electron collecting back electrode.^{5,18–19} External quantum efficiencies for these devices range from 0.02% up to about 1%, with open circuit voltages of 0.8–1.7 V and fill factors up to only 25%. In contrast, similar devices that use TiO₂ as the anode and either Au (Ref. 7 and this work) or Hg (Ref. 11) as the cathode produce quantum efficiencies of 1.5–6.4% and fill factors of up to 52% for similar open circuit voltages ranging from 0.7–1.1 V. The difference between these two approaches which leads to better efficiencies and fill factors is the direction of the internal field with respect to that of the incident light.

In a cell consisting of ITO/polymer/Al (or Mg or Ca), the internal field created by the difference in electrode work functions is such that holes exit through the ITO and electrons are drawn to the opposite electrode when operating in open circuit mode. As discussed earlier, a majority of the light will be absorbed at the incident electrode. For light incident through the semitransparent ITO, holes will immediately exit through the ITO while electrons must travel through the entire polymer layer to reach the opposite electrode [Fig. 9(b)]. Low electron mobilities in these polymers, on the order of 10^{-9} cm²/Vs, lead to lower efficiencies and fill factors. In contrast, the ITO/TiO₂/polymer/Au (or Hg) devices have an internal field in the opposite direction such that the TiO₂ collects electrons and the holes go to the Au [Fig. 9(a)]. With light incident through the ITO/TiO₂ side, the greatest concentration of excitons are conveniently lo-

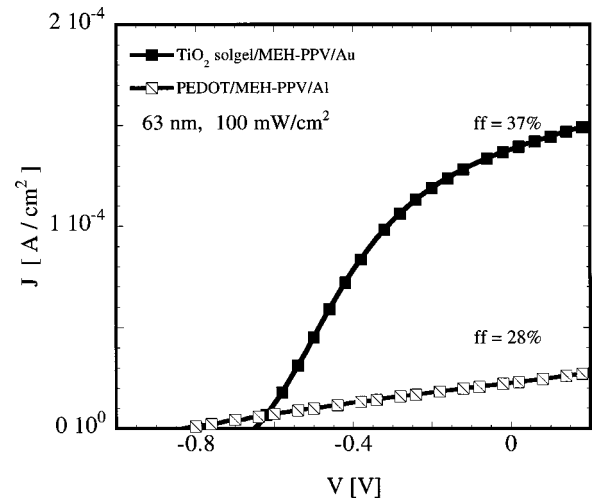


FIG. 10. Current density as a function of applied voltage comparing ITO/TiO₂ sol-gel/MEH-PPV/Au and ITO/PEDT/MEH-PPV/Al devices. MEH-PPV layer thickness is 63 nm and incident light intensity is 100 mW/cm².

cated next to the TiO₂/polymer dissociation interface. Once dissociation occurs, electrons are immediately transferred to the TiO₂ and the holes, with a relatively higher mobility, travel to the opposite electrode to exit the device. This effect contributes to the higher quantum efficiencies and fill factors. Figure 10 shows J - V curves comparing these two types of devices (ITO/TiO₂ sol-gel/MEH-PPV/Au and ITO/PEDT/MEH-PPV/Al) for 63-nm polymer layers. The ITO/PEDT/MEH-PPV/Al device has a short circuit current density an order of magnitude less than its TiO₂ counterpart, as well as a fill factor barely above 25%.

In addition, we compare our results to blends where the incorporation of an electron-transporting species improves exciton dissociation and electron mobility. Earlier device results using MEH-PPV and an electron transporting polymer CN-PPV achieved quantum efficiencies of 5%, similar to what we observe here.^{1,2} The use of semiconducting nanoparticles, such as C₆₀ or CdSe, leads to improved efficiencies of 12 and 29%, respectively, but only at very high concentration ($\sim 90\%$) of nanoparticles where the nanoparticle itself is making a significant contribution to the photocurrent.^{1,2} At lower concentrations ($\sim 50\%$), the quantum efficiencies of these devices are nearer to 6%, comparable to our non-blended results. These results suggest that except for at extremely high concentrations, a rough TiO₂ layer is as effective at dissociation of excitons as interpenetrating nanoparticle or polymer blends with ITO and Al electrodes. The advantage of the layered structure over the blended structure is that it allows for more efficient charge transport. Such a layered structure has been successfully constructed in non-MEH-PPV laminated devices, where quantum efficiencies approaching 29% have been reached.³

IV. CHARGE TRANSPORT MODEL FOR POLYMER PHOTOVOLTAICS

As models for understanding the quantum efficiency²⁰ and the energy conversion efficiency²¹ in polymer-based photo-

voltaics have been described recently, we focus here on a model for understanding the J - V characteristics of polymer-based photovoltaics. We consider the case of negligible reflection at the glass/polymer interface. The quantum efficiency η_q , i.e., the number of collected electrons divided by the number of incident photons, is a function of the electric field E and is given by

$$\eta_q(E) = \eta_D(E) * [1 - \exp(-\alpha L)],$$

where η_D is the exciton dissociation efficiency (the fraction of electron-hole pairs that contribute successfully to the current), α is the polymer absorption coefficient, and L is the thickness of the polymer film.

We next consider three contributions to the total current J , namely the injected current J_i caused by the thermally activated Schottky-like hole injection in the negative bias direction, the leakage current, J_1 caused by shorts through either the polymer or TiO₂ film, and the collected photogenerated current J_p . The total current density J is given by

$$J = J_i + J_1 + J_p,$$

where

$$J_i = A * T^2 \exp(qV_{bi}/kT) * [1 - \exp(-eV/kT)],$$

$$J_1 = G_1 V/A,$$

$$J_p = \eta_D(E) * [1 - \exp(-\alpha L)] e I_\nu / h \nu,$$

and where V_{bi} is the built-in potential equal to $\Phi_{TiO_2} - \Phi_{Au} = -0.8$ V, G_1 is the average conductance of the leakage path, A is the device area, and $I_\nu/h\nu$ yields the average number of photons per second as determined by the light intensity I_ν . The effective Richardson constant is $A^* = 16\pi\epsilon k^2 n_0 \mu / e^2$ where μ is the polymer hole mobility.²² We assume here that the voltage drop across the TiO₂ and the density of injected electrons are negligible, and that the mobility is constant with electric field. For the calculation of J_i , we cannot observe a significant difference between a linear and square-root dependence on voltage in the exponential; therefore we use the linear dependence for simplicity.

We also need to consider the electric field dependence of η_D . We assume a form consistent with our data which includes the $\mu\tau_r$ factor, namely the hole carrier mobility times the recombination time τ_r , where the average distance d before recombination is given by $\mu\tau_r(V - V_{bi})/L$. For this case,

$$\eta_D = \eta_{max} \{1 - \exp[-c\mu\tau_r(V - V_{bi})/L]\}, \quad V > V_{bi},$$

where c is a constant and η_{max} is the maximum dissociation efficiency. The short circuit current J_{sc} is therefore determined to be

$$J_{sc} = \eta_{max} \{1 - \exp[-c\mu\tau_r(V_{bi})/L]\} * [1 - \exp(-\alpha L)] e I_\nu / h \nu.$$

This form shows that J_{sc} increases with increasing mobility μ , recombination time τ_r , and light intensity I_ν . For this thickness range, J_{sc} decreases with increasing device thick-

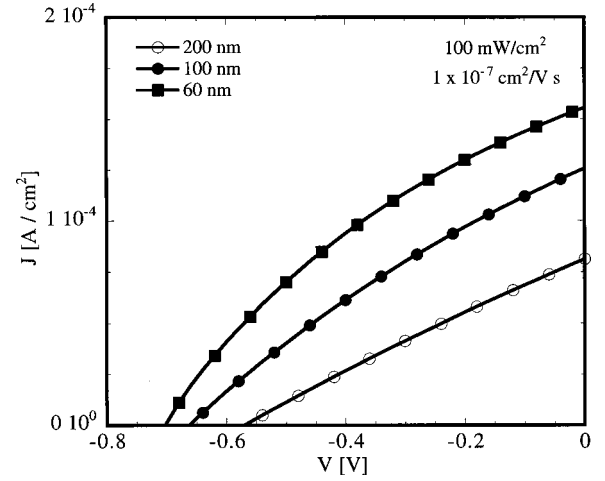


FIG. 11. Simulation of the current density as a function of applied voltage for a polymer photovoltaic at various thicknesses L of the polymer layer. The built-in potential is set constant at -0.8 V.

ness L because the exciton dissociation term dominates over the absorption term. We note that J_{sc} is independent of both leakage and carrier injection.

More fundamentally, we consider the effects that the polymer thickness, light intensity I_ν , mobility and leakage conductance G_1 have on the fill factor, and therefore the power efficiency, of the device. In Figs. 11–13, we graph J versus V for a series of simulated data using the equations above as a function of polymer thickness, light intensity, and mobility. We have taken realistic values for the polymer thickness (from 60 to 200 nm), light intensity (up to 100 mW/cm²), and the polymer hole mobility (1×10^{-7} – 1×10^{-6} cm²/V s). We have fixed V_{bi} to -0.8 V, consistent with the work function differences of our device structure. The simulations reproduce the data shown in Figs. 2, 3, and 5 remarkably well. Most notably, the simulations reveal the increase in fill factor that occurs with increasing mobility and decreasing polymer thickness. In addition, the data predicts the increase

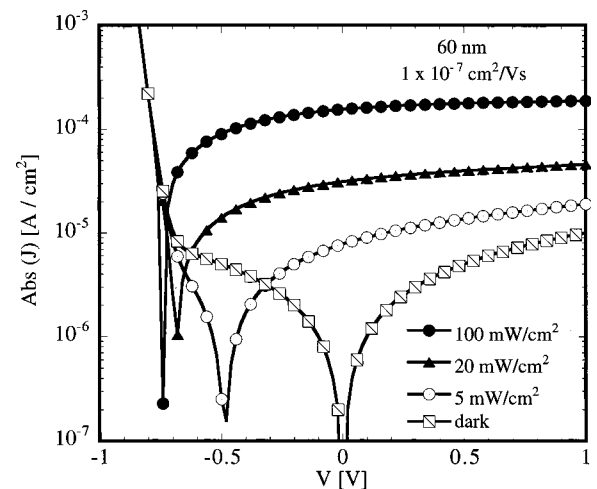


FIG. 12. Simulation of the absolute current density as a function of applied voltage for a polymer photovoltaic at various light intensities I . The built-in potential is set constant at -0.8 V.

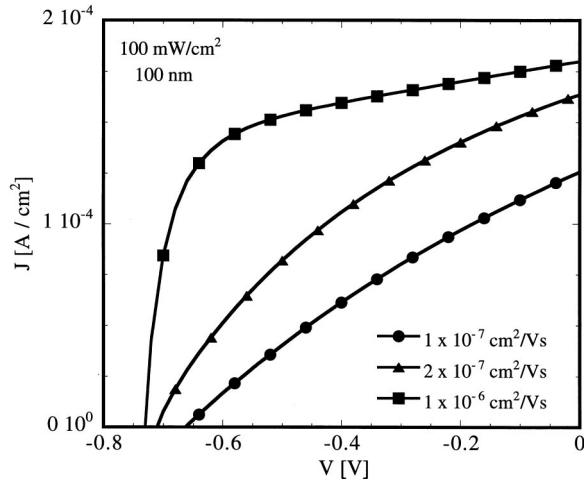


FIG. 13. Simulation of the current density as a function of applied voltage for a polymer photovoltaic at various polymer mobilities μ . The built-in potential is set constant at -0.8 V.

in V_{oc} that occurs with increasing light intensity. In Fig. 14, the effect of increasing leakage conductance between 1×10^{-5} and $5 \times 10^{-4} \Omega^{-1}$ is shown. We observe a substantial decrease in the fill factor and open circuit voltage with increasing leakage, and find that the leakage current dominates the current-voltage characteristics for leakage conductances much above $5 \times 10^{-4} \Omega^{-1}$. This result is consistent with our experimental results on devices exhibiting partial shorting. This dependence on the leakage current demonstrates the importance of good film quality for improved device performance.

Finally, we note the failures of the model. Most notable here is the dependence on the light intensity, as shown in Fig. 12. Here, the model fails to predict the decrease in fill factor with increasing light intensity, and it overestimates J_{sc} at low light intensities. This latter inconsistency could be due to charge trapping effects that predominate over the current at sufficiently low light intensities. These disagreements between our model and experiment may also be due to the oversimplified assumptions and omissions mentioned above. The electron mobility, surface recombination, field-dependent mobility, charge trapping, and voltage drop across the TiO_2 and polymer are only some of the factors which need to be studied and incorporated into the simulation. Nonetheless, this simplified model captures most of the salient features of our results on a wide variety of PPV-based polymer photovoltaics. Temperature-dependent current-voltage curves would further test the validity of this model.

Finally, we consider methods to improve the energy conversion efficiency in polymer-based solar cells. Clearly, the photogenerated current can be increased by increasing the fraction of dissociated carriers, as achieved in blended samples that induce phase separation on nanometer length scales; however, such blending will not necessarily improve the mobility and therefore will limit the fill factor and con-

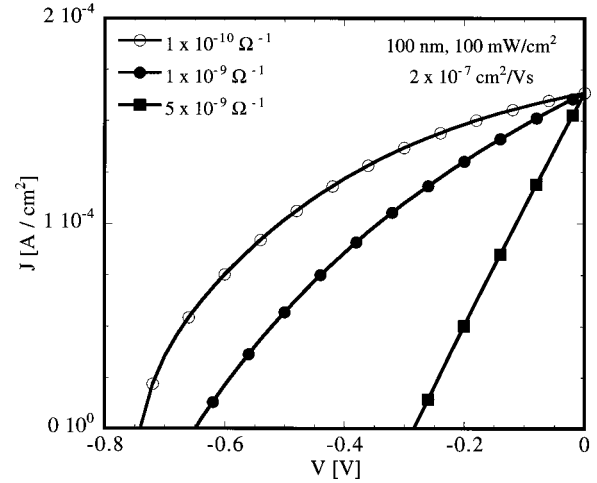


FIG. 14. Simulation of the current density as a function of applied voltage for a polymer photovoltaic at various leakage conductivities G_1 through the polymer film. The built-in potential is set constant at -0.8 V.

version efficiency at high light intensities. New materials that have high mobility charge separation moieties incorporated into the backbone should enable higher conversion efficiencies to be achieved. For example, a TPA-PPV-based device, which has a similar structure to MEH-PPV but also contains a high mobility TPA arylamino side group, has a quantum efficiency exceeding 25% in nonblended materials combined with fill factors near 50% at high light intensity.⁷ The results are comparable to the best conversion efficiencies found for blended samples. Finally, we note that if the TiO_2 electron mobility can be increased or the work function improved, higher fill factors and open circuit voltages would likely result.

V. CONCLUSIONS

In summary, we have studied the photovoltaic properties of solar cells that use a titanium dioxide layer as a semitransparent anode in conjunction with the photoactive polymer MEH-PPV. We have examined the effect of varying factors such as polymer thickness, polymer mobility, and TiO_2 morphology and have shown that thinner, higher mobility polymer layers combined with rough TiO_2 surfaces lead to the most efficient collection of photogenerated carriers. By using large surface area TiO_2 layers as a semitransparent electrode with a polymer and opposing electrode of favorable energy levels, we are able to reduce charge injection and achieve improved fill factors and an order of magnitude increase in external quantum efficiencies. We describe our results using simple models of charge transport in polymer semiconductors where the total current density is a function of the injected current at the metal-polymer interface, the leakage current through the polymer film, and the collected photogenerated current that results from the effective dissociation of excitons.

- * Author to whom correspondence should be addressed. Email address: sacarter@cats.ucsc.edu
- ¹J. J. M. Halls, C. A. Walsh, N. C. Greenham, E. A. Marseglia, and R. H. Friend, *Nature (London)* **376**, 498 (1995); J. J. M. Halls, K. Pichler, R. H. Friend, S. C. Moratti, and R. H. Friend, *Appl. Phys. Lett.* **68**, 3120 (1996); N. C. Greenham, X. G. Peng, and A. P. Alivisatos, *Phys. Rev. B* **54**, 17 628 (1996).
 - ²G. Yu, J. Gao, J. C. Hummelen, F. Wudl, and A. J. Heeger, *Science* **1995**, 270 (1789); G. Yu and A. J. Heeger, *J. Appl. Phys.* **78**, 4510 (1995).
 - ³M. Granström, K. Petritsch, A. C. Arias, A. Lux, M. R. Anderson, and R. H. Friend, *Nature (London)* **395**, 257 (1998); A. C. Arias *et al.*, *Phys. Rev. B* **60**, 1854 (1999).
 - ⁴B. O'Regan and M. Gratzel, *Nature (London)* **353**, 737 (1991).
 - ⁵For a discussion of the effects of water and oxygen on polymer-based photovoltaics, see N. Chawdhury, A. Kohler, M. G. Harrison, D. H. Hang, and R. H. Friend, *Synth. Met.* **102**, 871 (1999).
 - ⁶L. Bozano, S. A. Carter, J. C. Scott, G. G. Malliaras, and P. J. Brock, *Appl. Phys. Lett.* **74**, 1132 (1999).
 - ⁷A. C. Arango, L. Johnson, H. Horhold, Z. Schlesinger, and S. A. Carter, *Adv. Mater.* **12**, 1689 (2000).
 - ⁸Doped PEDT is Baytron P, provided by Bayer Corporation. For details, see S. A. Carter, J. C. Scott, and P. J. Brock, *Appl. Phys. Lett.* **71**, 1145 (1997).
 - ⁹The optical power output over the solar spectrum is determined using a calibrated silicon photodetector. Due to uncertainties in reflections and alignment, we estimate an error of $\pm 20\%$ for this calibration.
 - ¹⁰A. C. Arango, P. J. Brock, and S. A. Carter, *Appl. Phys. Lett.* **74**, 1698 (1999).
 - ¹¹T. J. Savenije, J. M. Warman, and A. Goossens, *Chem. Phys. Lett.* **287**, 148 (1998).
 - ¹²K. Petritsch and R. H. Friend, *Synth. Met.* **102**, 976 (1999).
 - ¹³A. Loannidis, J. S. Faoui, and M. A. Abkowitz, *J. Appl. Phys.* **84**, 1439 (1998).
 - ¹⁴The TiO₂ nanoparticles were provided by Solaronix.
 - ¹⁵K. Kajihara, K. Tanaka, K. Hirao, and N. Soga, *Jpn. J. Appl. Phys., Part 1* **35**, 6110 (1996).
 - ¹⁶P. A. van Hal, M. P. T. Christiaans, M. M. Wienk, and J. M. Kroon, *J. Phys. Chem. B* **103**, 4352 (1999).
 - ¹⁷J. S. Salafsky, *Phys. Rev. B* **59**, 10 885 (1999).
 - ¹⁸R. N. Marks, J. J. M. Halls, D. D. C. Bradley, and R. H. Friend, *J. Phys.: Condens. Matter* **6**, 1379 (1994).
 - ¹⁹J. J. Dittmer, K. Petritsch, E. A. Marseglia, and R. H. Friend, *Synth. Met.* **102**, 879 (1999).
 - ²⁰M. G. Harrison, J. Gruner, and G. C. W. Spencer, *Phys. Rev. B* **55**, 7831 (1997).
 - ²¹Katsumi Yoshino, Kazuya Tada, Akihiko Fujii, Esther M. Conwell, and Anvar A. Zakhidov, *IEEE Trans. Electron Devices* **44**, 1315 (1997).
 - ²²The Richardson constant A^* is different for polymer semiconductors than for inorganic semiconductors. For a detailed calculation, see J. C. Scott and G. G. Malliaras, *Chem. Phys. Lett.* **299**, 115 (1999).